Available online at www.sciencedirect.com

SciVerse ScienceDirect

Ceramics International 39 (2013) 6953–6961

CERAMICS INTERNATIONAL

www.elsevier.com/locate/ceramint

Opto-electronic properties of molybdenum doped indium tin oxide nanostructured thin films prepared via sol–gel spin coating

Saeed Mohammadi[a], Hossein Abdizadeh[a,b], Mohammad Reza Golobostanfard[a,*]

[a]School of Metallurgy and Materials Engineering, College of Engineering, University of Tehran, PO Box 11155-4563, Tehran, Iran
[b]Center of excellence for high performance materials, University of Tehran, PO Box 11155-4563, Tehran, Iran

Received 30 December 2012; received in revised form 12 February 2013; accepted 13 February 2013
Available online 20 February 2013

Abstract

Molybdenum-doped indium tin oxide thin films were synthesized using sol–gel spin coating technique. The influence of different molybdenum-dopant contents on the electrical, optical, structural, and morphological properties of the films were characterized by means of four point probe, UV–Vis–IR spectroscopy, X-ray diffraction, field emission scanning electron microscopy, and atomic force microscopy. For this purpose, addition of different molybdenum contents with tin at a fixed 6 at% is considered as the first approach. For the second and third approaches, different molybdenum-doping contents were added at a constant atomic ratios of In:Sn=94:6 and In:Sn=95:5, respectively. Obtained results indicate that minimum resistivity of $22.3\times10^{-3}\,\Omega\,cm$ and optical transmittance of more than 80% in the UV–Vis–IR region with a band gap of 3.83 eV were achieved for the films prepared through the first approach at molybdenum and tin doping contents of 0.5 and 5.5 at%, respectively. X-ray diffraction analysis confirmed the formation of cubic bixbyite structure of indium oxide and rhombohedral structure of indium tin oxide for molybdenum-doped films with small shift in a major peak position to lower diffraction angles with the addition of molybdenum. Field emission scanning electron microscopy micrographs do not show any specific changes in grain size of the films with addition of molybdenum beside tin. Atomic force microscopy studies show that the addition of molybdenum at optimum content to indium tin oxide films results in the formation of films with compact surface and less average roughness than the undoped indium tin oxide films.

Keywords: Indium tin oxide; Molybdenum; Sol–gel spin coating; Opto-electronic properties

1. Introduction

Transparent conductive oxide (TCO) thin films with low electrical resistivity and high optical transmittance have caused a great deal of interest due to their wide applications in opto-electronic fields such as dye synthesized solar cells [1], liquid crystal displays [2,3], organic light emitting diodes [4], and also for gas sensing devices [5]. Among the various available TCOs such as fluorine doped tin oxide (FTO), aluminum doped zinc oxide (AZO), and antimony doped tin oxide (ATO), the best known is tin doped indium oxide (ITO) due to its considerable characteristics of high optical transmittance, high conductivity, and chemical stability [6–8]. Although ITO is the most considered TCOs, research on improving electrical and optical properties of indium oxide (In_2O_3) based materials is continuing [9,10]. In recent years, more attention on TCO materials has been considered on the achievement of good compromise between electrical conductivity and transparency in the visible range. In this regard, recent research has shown that the opto-electronic properties of thin films were highly influenced by the nature and content of the added impurity rather than by optimization of preparation parameters such as annealing temperature and thickness of the films [11]. Based on the literature, different impurities have been doped into the In_2O_3 matrix, including tin (Sn), gallium (Ga), copper (Cu), zirconium (Zr), zinc (Zn), and titanium (Ti) [12–17]. Compared to those, Mo-dopant has more efficiency as it can add three electrons to the free carriers due to the high valence difference between Mo^{+6} ions and substituted In^{+3} ions, which successfully leads to

*Corresponding author. Tel.: +98 91 22300382; fax: +98 21 88006076.
E-mail address: Mohammadreza.Golbostanfard@gmail.com (M.R. Golobostanfard).

0272-8842/$ - see front matter © 2013 Elsevier Ltd and Techna Group S.r.l. All rights reserved.
http://dx.doi.org/10.1016/j.ceramint.2013.02.032

the development of Mo-doped In_2O_3 (IMO) thin films. Moreover, IMO thin films possess fewer defect centers due to addition of low Mo-dopant content compared with the other doped In_2O_3-based thin films, which leads to decrease of free carrier absorption in the near-infrared (NIR) region, resulting in low impurity scattering. As reported in the literature, recent researches have mainly focused on the effect of oxygen partial pressure [18–24], annealing temperature [22], and thickness of the films [25] in the constant Mo-doping content as well as addition of different Mo-doping contents in In_2O_3 matrix in a constant preparation process [11,26–29] for the IMO thin films. More detailed investigations have revealed that these films are mostly prepared by magnetron sputtering [18–21], pulsed laser deposition [22,23], plasma evaporation [24,26], ion-beam assisted evaporation (IBAE) [25], and spray pyrolysis [27,29,30] methods.

Till now, no one has studied the effects of different Mo-doping contents as a co-dopant beside Sn on the opto-electronic and microstructural properties of In_2O_3 thin films with any available methods. Considering the excellent properties of Mo-dopant, it is worth investigating the addition of different Mo-doping contents in ITO thin films via sol–gel spin coating technique, in order to obtain new TCO with comparable opto-electronic properties with ITO thin films.

2. Material and methods

2.1. Sol preparation

The indium tin molybdenum oxide (ITMO) thin films were prepared via sol–gel spin coating technique using anhydrous $InCl_3$ (Alfa Aesar, 99.99%), $SnCl_2.2H_2O$ (Merck, $>98\%$), anhydrous $MoCl_5$ (Aldrich, 99.99%) as the precursors, acetylacetone (Merck, $>99\%$), and absolute ethanol (Merck, $>99\%$) as solvents. For this purpose, first $InCl_3$ was dissolved in acetylacetone, and the resultant solution (0.2 M) was refluxed at 85 °C for 1 h. Then, required amount of $SnCl_2.2H_2O$ was dissolved in absolute ethanol at room temperature (0.2 M) and added as Sn dopant to the above solution. The resultant sol was mixed and refluxed at 85 °C for 1 h until transparent ITO sol was achieved. Then, the required amount of $MoCl_5$ was dissolved in absolute ethanol (0.2 M) and added to the ITO sol. The obtained solution was then mixed and refluxed at 85 °C for another 1 h until a transparent ITMO sol was achieved. Finally, the obtained sol was aged for 1 day at room temperature. Three different approaches for addition of Mo-doping in the ITO ($In_3Sn_4O_{12}$) thin films were considered: (I) For the first approach, In content was considered at 94 at% and Mo was added beside Sn dopant at a fixed 6 at% with general formula of $In_3Sn_{4-x}Mo_xO_{12}$ and atomic percent of Mo–Sn: 0.25–5.75 (S_1), 0.5–5.5 (S_2), 1–5 (S_3), and 3–3 (S_4). In this approach the main purpose was to consider the substitution of the Sn with Mo in In_2O_3 lattice. (II) For the second approach, Mo was doped in ITO structure and its content was varied at 0.25 (S_5), 0.5 (S_6), and 1 at% (S_7) at a constant atomic ratio of In:Sn = 94:6 with general formula of $In_{3-x}Sn_{4-y}Mo_zO_{12}$ ($x+y=z$). In this approach Mo substitutes with both In lattice sites and Sn. (III) For the third approach, Mo was added at 0.25 (S_8) and 0.5 at% (S_9) at a constant atomic ratio of In:Sn = 95:5 with general formula the same as Approach II. In this approach the main goal was to consider the regions with higher In content than 94 at%. It is worth considering that our explanation that Mo dopant substitutes with Sn (Approach I) and also with In lattice sites and Sn (Approach II, III) is based on the most possibilities according to the detailed calculated composition of prepared samples in Table 1. However, there may be other possibilities including substitution of Mo dopant in oxygen vacancies, oxygen interstitials, and neutral impurities. The composition and obtained electrical resistivity of the undoped ITO thin films (S_0) and Mo-doped ITO samples are summarized in Table 1.

Table 1
Composition and electrical resistivity of the prepared ITMO thin films.

Sample	Composition				Resistivity $\times 10^{-3}$
	In	Sn	Mo	*Approach	(Ω cm)
S_0	94	6	–	Undoped ITO	59.2
S_1	94	5.75	0.25	I	31.22
S_2	94	5.5	0.5	I	22.3
S_3	94	5	1	I	85.5
S_4	94	3	3	I	256
S_5	93.77	5.98	0.25	II	49.1
S_6	93.53	5.97	0.5	II	37.8
S_7	93.05	5.95	1	II	196.4
S_8	94.77	4.98	0.25	III	38.25
S_9	94.53	4.97	0.5	III	26.8

*(I) Mo–Sn dopant: fixed at 6 at% of total In, Sn and Mo contents, (II) Mo added at fixed atomic ratio of In:Sn = 94:6 and (III) Mo added at fixed atomic ratio of In:Sn = 95:5.

2.2. Film preparation

Soda lime substrates were washed with a detergent and cleaned ultrasonically with deionized water and ethanol. Then, the prepared sol was deposited on the substrate using spin coating technique. Spin parameters, including spin speed and time, were fixed at 3000 rpm and 30 s, respectively. The coated substrates were heated at 200 °C after each step in order to dry the ITMO layers. Spinning and drying cycles were repeated in order to reach the desired film thickness. Finally, the as-deposited films were annealed at 500 °C in air atmosphere in electric furnace for 1 h. Fig. 1 shows the overall flow chart for ITMO thin films preparation via sol–gel spin coating technique.

2.3. Thin film characterization

The characteristics of nanostructured thin films were investigated by variety of analysis techniques. X-ray diffraction (XRD) patterns were obtained using an X-ray diffractometer, model Philips PW1730, with Cu K_α radiation ($\lambda = 1.5405$ Å,

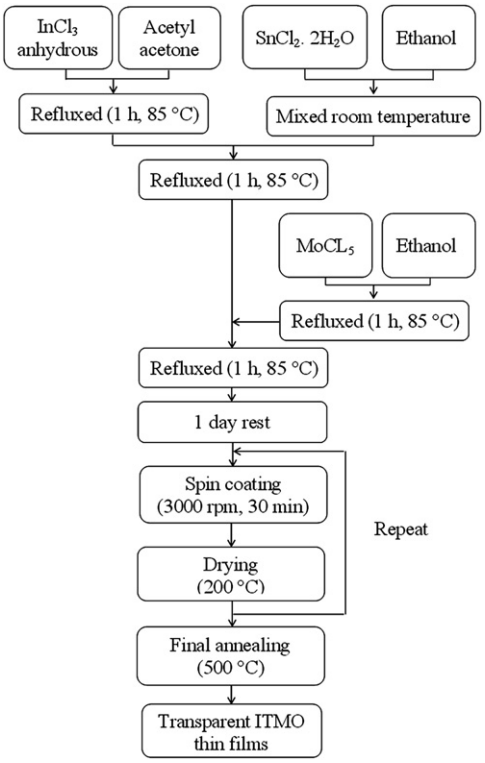

Fig. 1. A flow chart for ITMO thin films preparation.

40 kV, and 30 mA) in the range of 29–36° with step size of 0.02°. The mean particle size, morphologies, and surface roughness of the films were observed using field emission scanning electron microscopy (FESEM) model Hitachi S4160 and atomic force microscopy (AFM), model DME C26 operating in a non-contact mode. The resistivity of the films was measured by the four point probe method Keithly model 196 Sys-DMM 2 at room temperature. The transmission spectra and optical band gap in the UV–Vis–IR region (300–2500 nm wavelengths) were determined on a UV–Vis–IR Spectrophotometer Cary instrument, model 500i.

3. Results and discussions

3.1. Electrical properties

According to the literature, Sn dopant in In_2O_3 thin films shows the minimum electrical resistivity at 6 at% [12,31]. Therefore, the first two approaches are based on the addition of Mo beside Sn at a fixed 6 at% or addition of Mo at a constant atomic ratio of In:Sn = 94:6 in ITO structure. For the first approach, the prepared ITMO thin films (S_1–S_4 samples) can be located at position 1–4 in the In_2O_3–SnO_2–MoO_3 partial triple diagram in Fig. 2. The variation of sheet resistance and electrical resistivity for undoped ITO and ITMO thin films based on the selected approach are shown in Fig. 3.

Approach I. For the first approach, the electrical resistivity decreased with the increase in Mo-doping content and reached a minimum resistivity of $22.3 \times 10^{-3}\ \Omega$ cm for composition S_2. Further increase in Mo-doping content increases the resistivity so that the electrical resistivity of $256 \times 10^{-3}\ \Omega$ cm is obtained for composition S_4.

It was known that the Sn^{2+} ions transform to Sn^{4+} ions in an oxygen-rich environment [32]. Since all the samples were annealed in air at 500 °C, the Sn ions exist in the form of Sn^{4+}. Although there are other possible lower valence of Mo such as Mo^{3+}, Mo^{4+}, and Mo^{5+} with calculated ionic radius of about 0.69, 0.65, and 0.61 Å [33], Mo^{6+} valence state is more dominant as discussed in follows. Recent studies on high resolution XPS spectra for IMO films grown at 500 °C revealed that Mo exists in the oxidation states of +6 and +4 as well as an intermediate oxidation state of $+4 < x < +6$ [19]. Since in oxygen-rich media, Mo^{4+} is oxidized into Mo^{5+}, transient state firstly, and then Mo^{5+} forms the stable form Mo^{6+} by oxidation, the oxidation conditions leads to the dominance of the Mo^{+6} oxidation state. The presence of Mo in oxidation state of Mo^{+6} compared with other oxidation states in In_2O_3 films is widely reported in works of other authors [11,22,26–29].

The initial decrease in electrical resistivity with addition of Mo up to 0.5 at% can be explained as follows. As In content was considered at a fixed content of 94 at%, it is expected that Mo^{6+} substitutes mostly with Sn^{4+} rather than with In^{3+}. As a result, the valence difference of 2 between Mo^{6+} and Sn^{4+} would produce two free carriers per atomic substitution, leading to an increase of carrier concentration. Furthermore, recent studies in chemical character of impurity dopant element in TCO materials revealed that the mobility of doped In_2O_3 thin films increases strongly with increase in the Lewis acid strength of the doping element [34]. The Lewis acid strength (L) can be calculated using Zhang formula [35] as follows:

$$L = \frac{z}{r^2} - 7.7x_z + 0.8 \quad (1)$$

where r is the ionic radius of the ion, z is charge number of atomic core, and x_z is the electronegativity of the element in the respective oxidation state. Ionic radius, Lewis acid strength, and charge carrier difference of Mo^{6+}, Sn^{4+}, and In^{3+} ions are summarized in Table 2. According to this

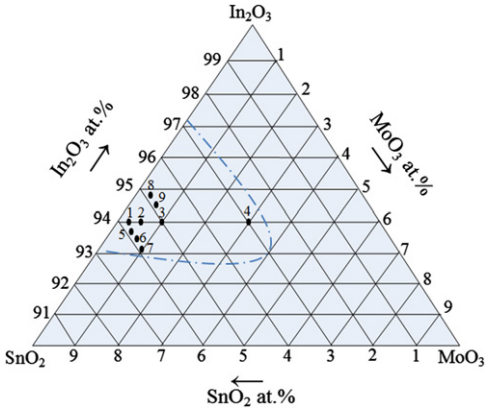

Fig. 2. In_2O_3–SnO_2–MoO_3 partial triple diagram.

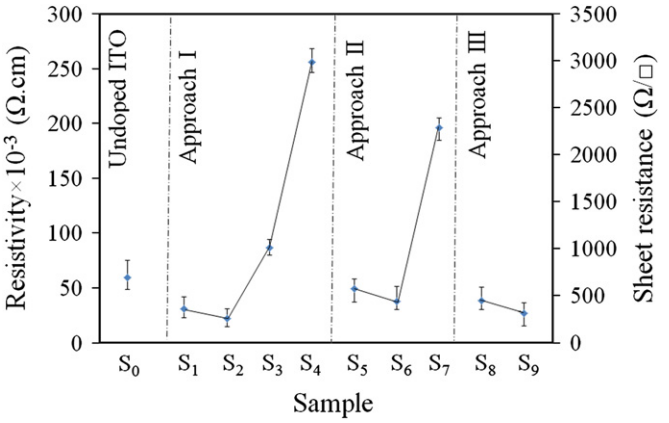

Fig. 3. Sheet resistance and electrical resistivity for undoped ITO (reference sample) and ITMO thin films based on the selected approach.

Table 2
Ionic radius, Lewis acid strength, and charge carrier difference between Mo^{6+}, Sn^{4+}, and In^{3+} ions.

Doping ions	Ionic radius (Å)	Lewis acid strength	Difference between free charge carrier with In^{3+}
Mo^{6+}	0.62	3.667	3
Sn^{4+}	0.71	0.228	1
In^{3+}	0.81	1.026	–

table, substitution of Sn^{4+} ions with Mo^{6+} ions increases both free carrier concentrations and Lewis acid strength of Mo-doped thin films, which ultimately enhance conductivity. However, there is more possibility of scattering when Mo^{6+} substitutes with Sn^{4+} ions due to higher difference between ionic radii of Mo^{6+} and In^{3+} compared with the ones between Sn^{4+} and In^{3+}. Considering these, it can be concluded that for low addition of Mo dopant content, the former reasons play a key role and decrease the electrical resistivity.

For higher Mo-dopant contents, the resistivity of the films increases due to solubility limit of Mo atoms in In_2O_3 lattice in sol–gel method. Similar trend with an increase of resistivity at higher Mo-dopant contents was also reported for the IMO thin films by Parthiban et al. [22,29]. Furthermore, increase of free carrier concentrations with the increase of Mo-doping content increases the electrical resistivity due to the increase of electron scattering and ionized impurity scattering. As a result, the minimum resistivity was achieved for the addition of Mo-doping at the optimum content of 0.5 at% for composition S_2.

Approach II. The second approach to investigate the effect of Mo-doping content on the electrical properties of the ITO films leads to investigation of electrical properties of ITMO films at position 5–7 in the In_2O_3–SnO_2–MoO_3 triple diagram with detailed composition of In:Sn:Mo = 93.77:5.98:0.25 (S_5), In:Sn:Mo = 93.53:5.97:0.5 (S_6), and In:Sn:Mo = 93.05:5.95:1(S_7), respectively. In this approach electrical properties of ITMO thin films with 3 at% of Mo-doping content were not considered due to maximum electrical resistivity which was achieved at a content higher than the solubility limit of Mo in In_2O_3 matrix in the sol–gel process. The undoped ITO thin films exhibited an resistivity of $59.2 \times 10^{-3}\ \Omega$ cm after which it decreased to a value of $37.8 \times 10^{-3}\ \Omega$ cm when Mo-doping level increased to 0.5 at%. In this approach, decrease of electrical resistivity with the increase of Mo-doping content can be attributed to the substitution of more Mo^{6+} with In^{3+} lattice sites compared with Sn^{4+}, as shown in the detailed composition of the prepared films in Table 1. As a result, substitution of Mo^{6+} with In^{3+} causes increase of free carrier concentration due to the large valence difference between Mo^{6+} ions and In^{3+} ions. Also, improvement in conductivity can be related to increase of mobility due to the substitution of Mo^{6+} ions with higher Lewis acid strength than substituted In^{3+} lattice ions and also with Sn^{4+}.

However, for higher Mo-doping levels (1 at%) the magnitude of electrical resistivity increased up to $196.4 \times 10^{-3}\ \Omega$ cm. This may be due to the fact that when the contents of Mo atoms increased, they probably do not occupy proper lattice sites in the In_2O_3 because of the solubility limit Mo in In_2O_3. In addition, increase in free carrier concentration at higher Mo- doping content increases both electron scattering and ionized impurity scattering, which significantly reduce the conductivity of the films.

Approach III. More detailed and comprehensive look at the location of selected points of prepared films in two previous considered approaches indicates that electrical properties of ITMO thin films were investigated at a fixed In content of 94 at% in the In_2O_3–SnO_2–MoO_3 triple diagram and the contents lower than it. To investigate the regions which are riches with In contents, the effect of Mo-doping content at 0.25 and 0.5 at%, with minimum electrical resistivity in two previous approaches was considered at a constant atomic ratio of In:Sn = 95:5. These points can be located at positions 8 and 9 in the In_2O_3–SnO_2–MoO_3 triple diagram with detailed composition of In:Sn:Mo = 94.77:4.98:0.25 (S_8) and In:Sn:Mo = 94.53:4.97:0.5 (S_9), respectively. In this approach, obtained results show that resistivity of the ITMO thin films decreased from $38.25 \times 10^{-3}\ \Omega$ cm for Mo-doping content of 0.25 at% to $26.8 \times 10^{-3}\ \Omega$ cm for Mo-doping content of 0.5 at%. Reduction of electrical resistivity can be explained as substitution of Mo^{6+} ions with In^{3+} lattice sites and also with Sn^{4+}, leading to increase of free carrier concentration, improvement of Lewis acid strength, and thereby improvement of conductivity. By considering detailed composition of prepared films in Approach II and III (Table 1) at constant Mo-doping content (samples S_5 and S_8, S_6 and S_9), it can be seen that Approach III has less Sn dopant and more In than Approach II. Theoretically, there is a higher possibility for substitution of Mo with In lattice sites than with Sn dopant sites. According to Table 2, there is a grater difference between Lewis acid strength and free carriers

of Mo^{6+} and In^{3+} than those of between Sn^{4+} and In^{3+}; therefore, it is expected that more conductivity is achieved by substitution of Mo^{6+} with In in In-rich regions. As a result, addition of Mo dopant in In-rich regions (Approach III) is more beneficial than in regions with lower In content (Approach II).

With regard to the minimum resistivity achieved for ITMO thin films in three considered approaches (S_2, S_6 and S_9), one can say that minimum electrical resistivity was achieved for addition of Mo-doping content of 0.5 at% in all prepared ITMO thin films. Considering this, the value of electrical resistivity decreased with addition of Mo beside Sn to lower degrees from the In_2O_3-based matrix (reference sample, S_0) to In:Sn:Mo=94.53:4.97:0.5 (Approach III, S_9), and decreased more until Mo–Sn doping contents reaches 6 at%, so that minimum resistivity was achieved for ITMO thin films at Mo–Sn doping contents of 0.5–5.5 at% (Approach I, S_2). Decrease in electrical resistivity of obtained ITMO thin films with addition of Mo-dopant beside Sn correlates well with decrease in electrical resistivity of ITGO thin films from undoped In_2O_3 to lower indium contents by adding Ge along with Sn in In_2O_3 thin films [36]. Further increase of Sn content, In:Sn:Mo=93.53:5.97:0.5 (Approach II, S_6), increases the resistivity of ITMO thin films to higher degrees compared with optimum Sn and Mo-doping contents of 5.5 and 0.5 at%.

In summary, the minimum value of electrical resistivity obtained for S_2 in Approach I can be attributed to the substitution of Sn^{4+} with Mo^{6+} ions compared with substitution of Mo^{6+} ions with In lattice sites and Sn (Approaches II and III). As mentioned before, it is noteworthy that substitution of Sn with Mo is preferable in this approach and up to 0.5 at% due to Sn low Lewis acid strength and also to its lower charge difference with In^{3+} compared with the ones for Mo. Therefore, it is expected that sample S_2 in Approach I has more conductivity compared with samples S_6 and S_9 in Approach II and III, in which Mo^{6+} substitutes with less Sn and more In lattice sites.

Considering that the optimum electrical resistivity for ITMO thin films was achieved in Approach I, the optical and microstructural properties of ITMO thin films were investigated in this approach with atomic percent of Mo–Sn: 0.25–5.75, 0.5–5.5, and 1–5, respectively.

3.2. Optical properties

Fig. 4 shows UV–Vis–IR transmittance spectra of undoped ITO and ITMO thin films with Mo-doping contents of 0.25, 0.5, and 1 at% beside Sn in the first approach. According to this figure, the optical transmittance of the ITMO thin films increased with increase of the Mo doping content until 0.5 at%, reached the maximum transmittance of more than 80% and then decreased to lower degrees with addition of Mo doping content. Moreover, for ITMO films the transparency extends further into the IR region, while for undoped ITO

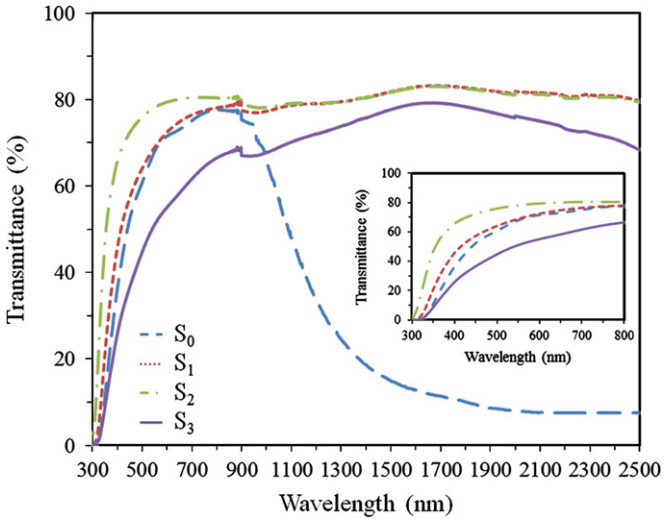

Fig. 4. UV–Vis–IR transmittance spectra of undoped ITO and ITMO thin films with different Mo doping contents of first approach.

films transparency reduced significantly. Recent research on high mobility TCOs revealed that Mo has lower free carrier absorption than Sn dopant does due to its higher mobility; consequently transparency of IMO thin films extends well into IR regions compared with the conventional ITO films, in which their transmittance spectra decreases in the IR region due to the high degree of free-carrier absorption. Thus, it is expected that substitution of Sn^{4+} with Mo^{6+} ions increases transmittance of Mo doped films to higher values at content lower than solubility limit of Mo in In_2O_3 lattice.

However, decrease in the optical transmittance of the ITMO films at higher Mo doping levels (1 at%) can be due to more electron scattering and ionized impurity scattering at higher carrier concentrations besides decrease in solubility limit of Mo in the In_2O_3 matrix, leading to increase of lattice distortion in some regions.

Fig. 5 shows the calculated optical band gap of the undoped ITO and ITMO films with different Mo-doping contents of the first approach. The optical band gap (E_g) was calculated from the relation between absorption coefficient (α) and photon energy ($h\upsilon$) using Tauc's equation as follows [37]:

$$(\alpha h\upsilon)^2 = A(h\upsilon - E_g) \quad (2)$$

where $h\upsilon$, A and E_g are photon energy, constant, and optical band gap of the thin films, respectively. The linear intercept of $h\upsilon$-axis gives the value of direct band gap. As can be seen, the optical band gap increased from 3.45 eV for the undoped ITO to 3.83 eV for ITMO thin films at Mo–Sn doping content of 0.5–5.5 at%, and decreased thereafter. The variation of the band gap can be explained as follows. Addition of Mo-doping contents up to 0.5 at% results in substitution of Sn^{4+} ions with Mo^{6+} ions, which will provide additional free carriers and cause the Fermi level to move into conduction band, causing an increase in the optical band gap, known as the Burnstein–Moss effect or blue shift [38]. On the other

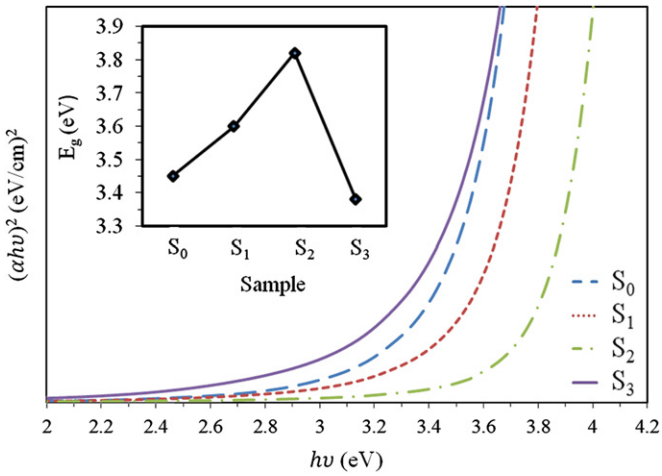

Fig. 5. The plot of $(\alpha h\upsilon)^2$ versus $h\upsilon$ for the undoped ITO and ITMO films with different Mo doping contents of first approach.

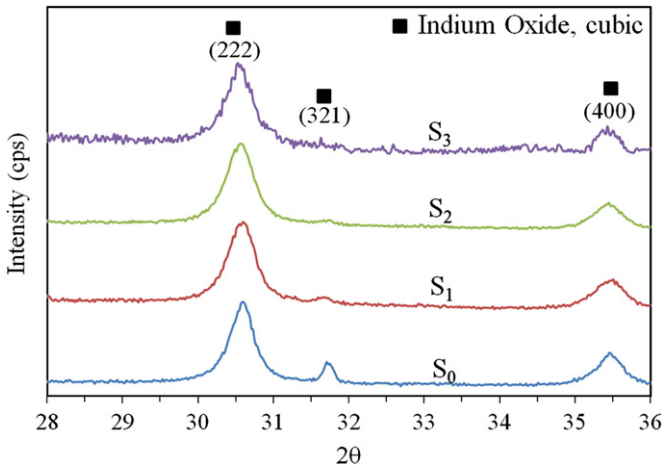

Fig. 6. XRD patterns of undoped ITO and ITMO films with Mo–Sn doping content of the first approach.

hand, at higher Mo-dopant contents (1 at%), the optical band gap decreased to 3.38 eV. Decrease of band gap can be explained as increase of electron–electron and electron–ionized donor interactions (lowering of conduction band edge), hole–hole interactions and hole–acceptor interactions (increase of valance band edge), and also electron–hole interactions. These interactions considerably decrease the band gap of highly doped semiconductors, known as the band gap renormalization [39].

The electrical properties of the films strongly depends on establishing good balance between free carrier concentration (n) and mobility (μ) of the films. Considering this, addition of Mo dopant into the based matrix In_2O_3 increases both carrier density and mobility of the films. It is noteworthy that increase of free carrier density up to the optimum level beside increase of mobility leading to improvement of electrical conductivity, while increase of carrier density more than the optimum level results in decrease of mobility and reduction of electrical conductivity.

Considering aforementioned criteria, the relationship between electrical and optical properties of ITMO films according to Mo doping content can be explained as: (I) Addition of Mo dopant to ITO films up to 0.5 at% increases both free carrier density and mobility of the films, resulting in increase of optical band gap, decrease of free carrier absorption and improvement of transparency of the films as can be seen in IR region in UV–Vis–IR spectra of the films (Fig. 4); (II) Addition of Mo dopant to ITO films more than 0.5 at% increases the free carrier concentration to a degree that results in decrease of mobility. This leads to decrease of optical band gap, increase of free carrier absorption and reduction of transparency of the films as can be seen in IR region in UV–Vis–IR spectra of the films (Fig. 4).

3.3. X-ray diffraction studies (XRD)

XRD patterns of ITMO films with different Mo-doping contents in the range of 0–1 at% beside Sn dopant in the first approach are shown in Fig. 6. For comparison, the XRD pattern of undoped ITO thin films at 6 at% of Sn was included. All of the patterns revealed that all of the crystalline peaks position in the XRD patterns agree fairly well with the values given in JCPDS file no. 06-0416 for the cubic bixbyite structure of In_2O_3 [40] and JCPDS file no. 88-0773 for the rhombohedral structure of ITO [41], without any trace of other crystalline peaks, indicating incorporation of Mo dopant besides Sn into the In_2O_3 lattice. As can be seen, the films are crystalline with the major peak position along the (2 2 2) plane. The position of the (2 2 2) peak shifted to lower diffraction angles with increase of Mo-doping content due to the difference between the ionic radii of Mo^{6+} ions and Sn^{4+} ions, indicating increase in lattice constant. Furthermore, this shift in the peak position with doping revealed the incorporation of Mo in the In_2O_3 structure in the presence of Sn. Also, it can be seen that the preferential orientation along (2 2 2) plane does not change to other peak position for Mo-doping content up to 1 at%. For higher Mo-doping contents (more than 1 at%), the preferential orientation is changed to (4 0 0) plane as reported by Parthiban et al. [22] and Prathap et al. [27].

3.4. Microstructural studies

Fig. 7 shows the FESEM micrograph of the undoped ITO and ITMO films with different Mo-doping contents. FESEM micrographs confirm the formation of nanostructured thin films with homogeneous and smooth surface with nearly spherical and fine-grained morphology. Additionally, the average grain size of prepared films was found to be in the range of 15–20 nm. According to the literature, when new dopant was added, the grain size of the films decreased due to increase of nucleation rates and interfacial energy; as a result, further crystal growth is inhibited [42]. However, in these samples the total amount of dopant is constant and the Sn was substituted with Mo, and no trend in grain size of the films can be observed with this substitution.

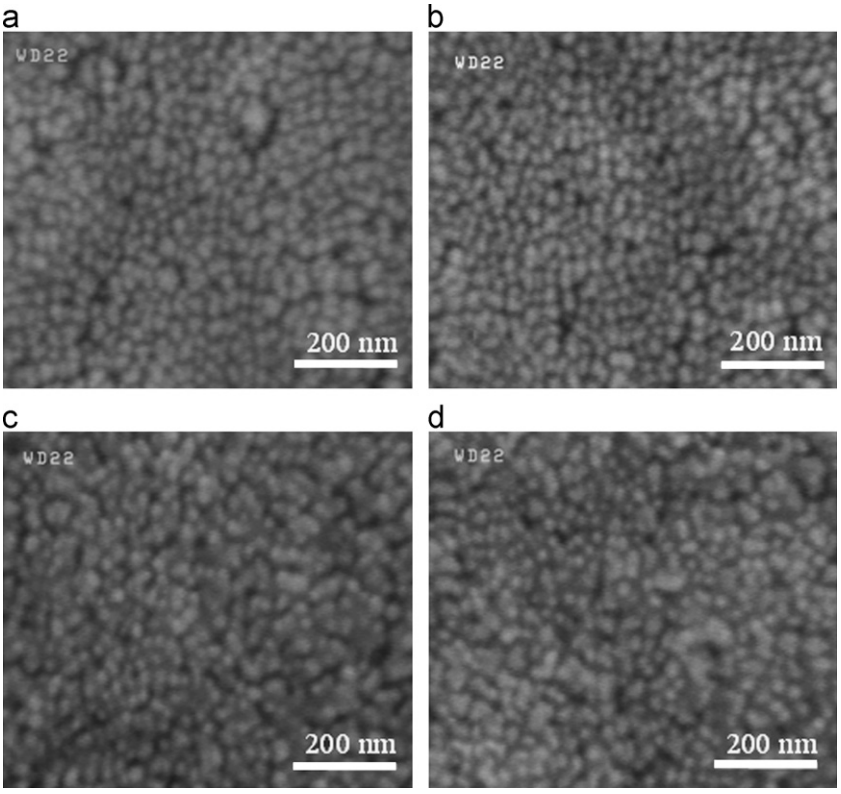

Fig. 7. FESEM micrographs of (a) undoped ITO thin films at 6 at% of Sn and ITMO thin films with Mo-doping content of (b) 0.25, (c) 0.5 and (d) 1 at% in the first approach.

3.5. AFM studies

Fig. 8 shows AFM images of the undoped ITO thin films with 6 at% of Sn dopant (S_0) and Mo-doped ITO thin films with optimum opto-electronic properties at Mo–Sn atomic content of 0.5–5.5 (S_2), respectively. For detailed morphological investigation, the root mean square (RMS) roughness (S_q) and the average roughness (S_a) parameters were calculated. These parameters are among two important factors for opto-electronic devices due to considerable importance of the surface morphology of the TCO electrode since it directly affects the surface morphology of materials deposited on it.

AFM images indicate the formation of crystalline thin films with uniform and smooth surface for undoped ITO thin films with average grain size of 25 nm and calculated average roughness of 10.23 nm and RMS roughness of 12.2 nm, while for Mo-doped ITO films at an optimum content, the size of grains, average roughness and RMS roughness of the film were found to be decreased to 15, 2.7, and 3.53 nm, respectively. It is evident that lower surface roughness with more compact surface was achieved for ITMO films by addition of Mo doping besides Sn at the optimum content to the In_2O_3 lattice. As can be seen, the more compact surface of the Mo-doped film can be attributed to its fine-grained microstructure compared with ITO film. Furthermore, the RMS roughness value achieved for ITMO thin films is lower than the commercially

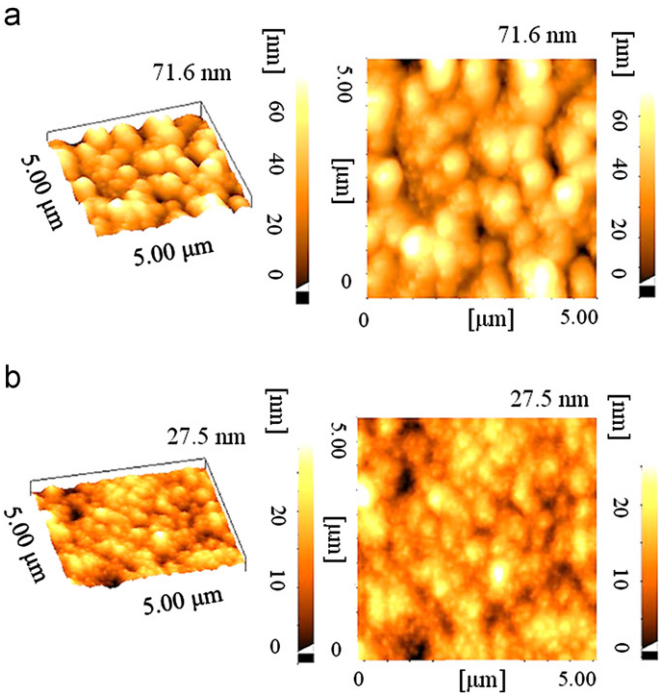

Fig. 8. Two and three dimensional AFM images for (a) undoped ITO (reference sample, S_0) and (b) Mo-doped ITO thin films with optimum opto-electronic properties (S_2).

available ITO films (~4 nm) [43]. Hence, the combination of more compact and homogenous surface with less average roughness provides new TCO with better opto-electronic

properties than ITO films for applications in opto-electronic devices.

4. Conclusions

Transparent conductive Mo-doped indium tin oxide (ITMO) nanostructured thin films have been synthesized successfully via sol–gel spin coating technique for the first time. The influences of different Mo-doping levels on the electrical, optical and microstructural properties of the films were investigated systematically. Obtained results indicate that better opto-electronic properties, including minimum electrical resistivity of $22.3 \times 10^{-3}\,\Omega\,\mathrm{cm}$ and optical transmittance of more than 80% in the UV–Vis–IR region with a band gap of 3.83 eV were achieved for the ITMO films prepared with atomic content of Mo–Sn: 0.5–5.5 at a fixed 6 at% compared with the undoped ITO thin films. Improvement of opto-electronic properties can be attributed to the substitution of Mo^{6+} ions with Sn^{4+} ions, leading to increase of free carriers and Lewis acid strength at contents less than solubility limit of Mo-dopant in the In_2O_3 lattice. Moreover, the IR transmittance of the ITMO films were completely developed compared to that of ITO films due to the high carrier mobility of these films. The XRD patterns indicate the formation of thin films with the cubic bixbyite structure of In_2O_3 and the rhombohedral structure of ITO for Mo-doped films, representing a small shift in major peak position to lower values and increase in lattice constant due to incorporation of Mo beside Sn into the In_2O_3 structure. However, in FESEM micrographs, no special trend in grain size of the films can be observed with substitution of Sn with Mo dopant. AFM images show that average roughness and RMS roughness parameters were reduced to lower values of 2.7 and 3.53 nm with addition of Mo at optimum content beside Sn to the In_2O_3 thin films.

References

[1] B. Pujilaksono, U. Klement, L. Nyborg, U. Jelvestam, S. Hill, D. Burgard, X-ray photoelectron spectroscopy studies of indium tin oxide nanocrystalline powder, Materials Characterization 54 (2005) 1–7.

[2] B.G. Lewis, D.C. Paine, Applications and processing of transparent conducting oxides, Materials Research Bulletin 25 (2000) 22–27.

[3] R.G. Gordon, Criteria for choosing transparent conductors, Materials Research Bulletin 25 (2000) 52–57.

[4] D. Lu, Y. Wu, J. Guo, G. Lu, Y. Wang, J. Shen, Surface treatment of indium tin oxide by oxygen-plasma for organic light-emitting diodes, Materials Science and Engineering: B 97 (2003) 141–144.

[5] Y.F. Sun, S.B. Liu, F.L. Meng, J.Y. Liu, Z. Jin, L.T. Kong, J.H. Liu, Metal oxide nanostructures and their gas sensing properties: a review, Sensors 12 (2012) 2610–2631.

[6] A. Beaurain, D. Luxembourg, C. Dufour, V. Koncar, B. Capoen, M. Bouazaoui, Effects of annealing temperature and heat-treatment duration on electrical properties of sol–gel derived indium-tin-oxide thin films, Thin Solid Films 516 (2008) 4102–4106.

[7] N.M. Torkaman, Y. Ganjkhanlou, M. Kazemzad, H.H. Dabaghi, M. Keyanpour-Rad, Crystallographic parameters and electro-optical constants in ITO thin films, Materials Characterization 61 (2010) 362–370.

[8] H. Cho, Y.H. Yun, Characterization of indium tin oxide (ITO) thin films prepared by a sol–gel spin coating process, Ceramics International 37 (2011) 615–619.

[9] W.C. Chang, S.C. Lee, C.H. Yang, T.C. Lin, Opto-electronic properties of chromium doped indium-tin-oxide films deposited at room temperature, Materials Science and Engineering: B 153 (2008) 57–61.

[10] S. Mohammadi, H. Abdizadeh, M.R. Golobostanfard. Effect of niobium doping on opto-electronic properties of sol–gel based nanostructured indium tin oxide thin films, http://dx.doi.org/10.1016/j.ceramint.2012.11.027.

[11] S. Kaleemulla, N.M. Rao, M.G. Joshi, A.S. Reddy, S. Uthanna, P.S. Reddy, Electrical and optical properties of In_2O_3: Mo thin films prepared at various Mo-doping level, Journal of Alloys and Compounds 504 (2010) 351–356.

[12] S. Seki, Y. Sawada, M.H. Wang, H. Lei, Y. Hoshi, T. Uchida, Electrical properties of tin-doped indium oxide thin films prepared by a dip coating, Ceramics International 38 (2012) S613–S616.

[13] L. Kong, J. Ma, F. Yang, C. Luan, Z. Zhu, Preparation and characterization of $Ga_{2x}In_{2(1-x)}O_3$ films deposited on ZrO_2 (1 0 0) substrates by MOCVD, Journal of Alloys and Compounds 499 (2010) 75–79.

[14] M. Sasaki, K. Yasui, S. Kohiki, H. Deguchi, S. Matsushima, M. Oku, T. Shishido, Cu doping effects on optical and magnetic properties of In_2O_3, Journal of Alloys and Compounds 334 (2002) 205–210.

[15] Y.C. Liang, Surface morphology and conductivity of zirconium-doped nanostructured indium oxide films with various crystallographic features, Ceramics International 36 (2010) 1743–1747.

[16] N. Ito, Y. Sato, P.K. Song, A. Kaijio, K. Inoue, Y. Shigesato, Electrical and optical properties of amorphous indium zinc oxide films, Thin Solid Films 496 (2006) 99–103.

[17] K. Gupta, K. Ghosh, S.R. Mishra, P.K. Kahol, Opto-electrical properties of Ti-doped In_2O_3 thin films grown by pulsed laser deposition, Applied Surface Science 253 (2007) 9422–9425.

[18] E. Elangovan, G.G. Alves, R. Martins, E. Fortunato, RF sputtered wide work function indium molybdenum oxide thin films for solar cell applications, Solar Energy 83 (2009) 726–731.

[19] Y. Yoshida, T.A. Gessert, C.L. Perkins, T.J. Coutts, Development of radio-frequency magnetron sputtered indium molybdenum oxide, Journal of Vacuum Science & Technology A-Vacuum Surfaces And Films 21 (2003) 1092–1097.

[20] X. Li, W. Miao, Q. Zhang, L. Huang, Z. Zhang, Z. Hua, The electrical and optical properties of molybdenum-doped indium oxide films grown at room temperature from metallic target, Semiconductor Science and Technology 20 (2005) 823–828.

[21] M.F.A.M. Van Hest, M.S. Dabney, J.D. Perkins, D.S. Ginley, High-mobility molybdenum doped indium oxide, Thin Solid Films 496 (2006) 70–74.

[22] S. Parthiban, V. Gokulakrishnan, K. Ramamurthi, E. Elangovan, R. Martins, E. Fortunato, R. Ganesan, High near-infrared transparent molybdenum-doped indium oxide thin films for nanocrystalline silicon solar cell applications, Solar Energy Materials and Solar Cells 93 (2009) 92–97.

[23] D. Ginley, B. Roy, A. Ode, C. Warmsingh, Y. Yoshida, P. Parilla, C. Teplin, T. Kaydanova, A. Miedaner, C. Curtis, A. Martinson, T. Coutts, D. Readey, H. Hosono, C.L. Perkins, Non-vacuum and PLD growth of next generation TCO materials, Thin Solid Films 445 (2003) 193–198.

[24] SS.Y. Sun, J.L. Huang, D.F. Lii, Effects of oxygen contents on the electrical and optical properties of indium molybdenum oxide films fabricated by high density plasma evaporation, Journal of Vacuum Science & Technology A-Vacuum Surfaces And Films 22 (2004) 1235–1241.

[25] R.K. Gupta, K. Ghosh, R. Patel, P.K. Kahol, Effect of thickness on optoelectrical properties of Mo-doped indium oxide films, Applied Surface Science 255 (2008) 3046–3048.
[26] S.Y. Sun, J.L. Huang, Properties of indium molybdenum oxide films fabricated via high-density plasma evaporation at room temperature, Journal of Materials Research 20 (2005) 247–255.
[27] P. Prathap, G.G. Devi, Y.P.V. Subbaiah, V. Ganesan, K.T.R. Reddy, J. Yi, Preparation and characterization of sprayed In_2O_3:Mo films, Physica Status Solidi A Applications and Material Science 205 (2008) 1947–1951.
[28] R.K. Gupta, K. Ghosh, S.R. Mishra, P.K. Kahol, Structural, Optical and electrical characterization of highly conducting Mo-doped In_2O_3 thin films, Applied Surface Science 254 (2008) 4018–4023.
[29] S. Parthiban, K. Ramamurthi, E. Elangovan, R. Martins, E. Fortunato, Spray deposited molybdenum doped indium oxide thin films with high near infrared transparency and carrier mobility, Applied Surface Science 94 (2009) 212101–212103.
[30] D.J. Seo, S.H. Park, Structural, electrical and optical properties of In_2O_3:Mo films deposited by spray pyrolysis, Physica B: Condensed Matter 357 (2005) 420–427.
[31] S. Seki, Y. Sawada, M. Ogawa, M. Yamamoto, Y. Kagota, A. Shida, M. Ide, Highly conducting indium-tin-oxide transparent films prepared by dip-coating with an indium carboxylate salt, Surface and Coatings Technology. 169-170 (2003) 525–527.
[32] K. Dhananjay, C.W. Chu, C.W. Ou, M.C. Wu, Z.Y. Ho, K.C. Ho, S.W. Lee, Complementary inverter circuits based on p-SnO_2 and n-In_2O_3 thin film transistors, Applied Physics Letters 92 (2008) 232103–232105.
[33] A. Kelly, K.M. Knowles, Crystallography and Crystal Defects, second ed., John Wiley & Sons, 2012.
[34] S. Calnan, A.N. Tiwari, High mobility transparent conducting oxides for thin film solar cells, Thin Solid Films 518 (2010) 1839–1849.
[35] Y. Zhang, Electronegativities of elements in valence states and their applications. 1. electronegativities of elements in valence states, Inorganic Chemistry 21 (1982) 3886–3889.
[36] J. Salardennea, C. Marcel, Y. Xu, G. Couturier, Electron scattering mechanisms in ITGO (Sn+Ge doped In_2O_3) thin films for low emittance window coatings, European Physical Journal 3 (1998) 233–235.
[37] J. Tauc, Amorphous and Liquid Semiconductors, Plenum Press, New York, 1974.
[38] S.M. Park, T. Ikegami, K. Ebihara, P.K. Shin, Structure and properties of transparent conductive doped ZnO films by pulsed laser deposition, Applied Surface Science 253 (2006) 1522–1527.
[39] A. Walsh, J.L.F. Da Silva, S.H. Wei, Origins of band-gap renormalization in degenerately doped semiconductors, Physical Review B: Condensed Matter 78 (2008) 75211–75215.
[40] Powder Diffraction File, JCPDS-International Centre for Diffraction Data-ICDD, Philadelphia, Card no.06-0416, 1997.
[41] Powder Diffraction File, JCPDS-International Center for Diffraction Data, Philadelphia, Card no. 88-773, 1972.
[42] JJ.D. Bryan, D.R. Gamelin, Doped semiconductor nanocrystals: synthesis, characterization, physical properties and applications, Progress in Inorganic Chemistry 54 (2005) 47–126.
[43] R.K. Gupta, K. Ghosh, R. Patel, S.R. Mishra, P.K. Kahol, Effect of substrate temperature on opto-electrical properties of Nb-doped In_2O_3 thin films, Journal of Crystal Growth 310 (2008) 4336–4339.